

# New Mechanism of Collapse and Revival in Wave Packet Dynamics Due to Spin–Orbit Interaction \*

P. Rozmej<sup>a</sup>, W. Berej<sup>a</sup> and R. Arvieu<sup>b</sup>

<sup>a</sup>Theoretical Physics Department, University MCS, 20-031 Lublin, Poland

rozmej@tytan.umcs.lublin.pl

<sup>b</sup>Institut des Sciences Nucléaires, F 38026 Grenoble-Cedex, France

arvieu@frcpn11.in2p3.fr

November 14, 1996

## Abstract

This article discusses the properties of time evolution of wave packets in a few systems. Dynamics of wave packet motion for Rydberg atoms with the hierarchy of collapses and revivals is briefly reviewed. The main part of the paper focuses on the new mechanism of quantum recurrences in wave packet dynamics. This mechanism can occur in any physical system with strong enough spin–orbit interaction. We discuss here the *spin–orbit pendulum* effect that consists in different motions of subpackets with different spin fields and results in oscillations of a fraction of average angular momentum between spin and ordinary subspaces. The evolution of localized wave packets into toroidal objects and backwards (for other class of initial conditions) is also subject to discussion.

PACS number(s): 03.65.Sq, 03.65.Ge, 32.90+a

---

\*Presented at the XXXI Zakopane School of Physics, Zakopane, Poland, September 3 – 11, 1996.

# 1 Introduction

Recent advances in experimental techniques have resulted in rapidly growing attention to the dynamics of particular nonstationary states, wave packets. With tunable, short and intensive laser pulses a creation and analysis of such states in atomic and molecular systems became available. An extensive research by means of both theoretical and experimental methods has brought an understanding of the intriguing phenomena of a hierarchy of collapses and revivals for particularly prepared wave packets in Rydberg atoms [1-7] and in Jaynes-Cummings model (JCM) of quantum optics [8-12].

In hydrogen and hydrogenoid atoms electrons can be excited to a coherent mixture of many Rydberg states that move almost classically for many Kepler periods [1-5,7]. However due to a nonequidistant spectrum of energy levels wave packets undergo a sequence of spreadings, collapses and revivals during long term evolution. There exist several time scales for the revivals (reccurences). The shortest one is associated with the period of a classical motion, i.e. Kepler period, the other ones called  $t_{rev}$  and  $t_{sr}$  (revival and superrevival times respectively) arise from subtle quantum interference effects. The examples of such effects are described in more detail in Section 2.

In atomic systems the appropriate wave packet can be excited by a suitably chosen laser pulse [2,6]. The time evolution can be then probed by the following pulse after precisely measured time delay. Using additionally a circularly polarized electric field allows for a creation of electronics wave packets which are stationary [13,14]. In this case the wave packet motion is stabilized by a nonlinear coupling in the analogous way as orbits of Trojan asteroids are stabilized in the celestial mechanics [15].

Another interesting phenomenon already observed in quantum optics is an atomic analogue to a double-slit experiment [16]. Again in hydrogen or hydrogenoid atoms one can excite, by a pair of laser pulses with an appropriate time delay, two wave packets localized on the opposite sides of the orbit. Such a state is often called a 'Schrödinger cat state' as it is a mesoscopic size realization of the famous Schrödinger cat problem [17].

In the following sections 3 and 4 we discuss the new dynamical structures in wave packet motion. These new effects arise when the strong enough spin-orbit interaction is present in a physical system. In order to exhibit these effects in the most transparent way we have chosen the simple central potential in spherical harmonic oscillator form. This choice allows for the

factorization of the evolution operator into two parts and for considering the orbital motion and spin-orbit motion separately, as well as for finding analytical solutions for both motions. In section 3 we present the spin-orbit pendulum effect [18-20] which is most pronounced for circular orbits. Section 4 contains the discussion of linear trajectories for which spin-orbit interaction spreads (periodically) the initially spherical, well localized wave packet into a toroidal object, with a classical trajectory being the symmetry axis of the torus. Such behaviour of the wave packet has been presented here for the first time.

All these experimental and theoretical achievements enrich our understanding of the basic features of quantum mechanics.

## 2 Properties of Rydberg wave packets

The discussion presented in this section is in line of that of [3,5,7,22].

Consider a hydrogen atom prepared in such a way that the wave function is a superposition of bound-state eigenfunctions

$$\Psi(\vec{r}, t) = \sum_n c_n u_n(\vec{r}) \exp(-iE_n t/\hbar), \quad (1)$$

where coefficients  $c_n$  are not negligible only for rather narrow range of  $n$  around the mean value  $N$ . Obviously  $\int u_n^* u_s d\vec{r} = \delta_{ns}$  and  $\sum_n |c_n|^2 = 1$ . This sum converges, therefore a finite number of  $c_n$  makes it arbitrarily close to 1 and is sufficient to represent  $\Psi$  with arbitrary accuracy. Then any  $\Psi$  is arbitrarily close to a periodic function of time [23]. Let  $K$  be the common multiple of all  $n$  for which  $c_n$  are not neglected. Then  $\Psi$  has a period  $T_{cl}K^2$ . The recurrence with this period is exact, but if many levels contribute to the sum (1) the required time is enormously long. However, nearly exact recurrences occur considerably earlier. The assumption that weights  $c_n$  are strongly centered around a mean value  $N$  permits an expansion of the energy in a Taylor series

$$E_n \simeq E_N + E'_N (n - N) + E''_N (n - N)^2 + E'''_N (n - N)^3 + \dots, \quad (2)$$

where each prime on  $E_N$  denotes a derivative. The derivative terms in (2) define distinct time scales that depend on  $N$ :  $T_{cl} = 2\pi N^3$ ,  $t_{rev} = (N/3 + 1/2) T_{cl}$ ,  $t_{sr} = (N^2/4 + 1/2) T_{cl}$ , called classical period, revival time

and superrevival time, respectively. Keeping terms through third order and disregarding an overall time-dependent phase, one can rewrite (1) as

$$\Psi(\vec{r}, t) = \sum_n c_n u_n(\vec{r}) \exp \left[ -2\pi i \left( \frac{(n-N)t}{T_{cl}} + \frac{(n-N)^2 t}{t_{rev}} + \frac{(n-N)^3 t}{t_{sr}} \right) \right]. \quad (3)$$

The convenient measure of the degree of recurrences is the recurrence probability (also referred to as autocorrelation function), where  $w_n = |c_n|^2$  and time units are atomic units,

$$P(t) = |\langle \Psi(0) | \Psi(t) \rangle|^2 = \sum_n w_n e^{it/n^2}. \quad (4)$$

In order to exhibit some properties of short term and long term evolution let us construct in a standard way the so-called circular wave packet [1-4]. Then we can choose  $c_n = (2\pi\sigma)^{-1/4} \exp[-((n-N)/2\sigma)^2]$  and  $u_n(\vec{r}) = \Phi_{n,n-1,n-1}(\vec{r})$  (aligned standard hydrogenic eigenfunction with  $l = m = n-1$ ). The features of the evolution of such a circular wave packet are illustrated below with some numerical examples. We show the results obtained for the wave packet with  $N = 60$ ,  $\sigma = 1.5$  and the summation over  $n$  taken from  $n_1 = 50$  to  $n_2 = 70$ . For this case  $t_{rev} = 20.5 T_{cl}$ ,  $t_{sr} = 900.5 T_{cl}$  and the mean principal quantum number  $N$  is large enough for the fractional revivals to appear.

The short term evolution (time range 0–50  $T_{cl}$ ) is displayed in Fig. 1, where the recurrence probability (4) is plotted as function of time. Initial peak intensity decreases very fast, and it is seen that after 4 revolutions wave packet is well spread over the whole orbit. Around  $t \simeq 5 T_{cl}$  (1/4 of  $t_{rev}$ ) peaks appear 4 times more frequently indicating formation of a fractional revival of 1/4 order (see also Fig. 3b). Around  $t \simeq 7 T_{cl}$  (1/3 of  $t_{rev}$ ) and  $t \simeq 10 T_{cl}$  (1/2 of  $t_{rev}$ ) the frequency of peaks of the autocorrelation function indicate formations of the fractional revivals of orders 1/3 and 1/2, respectively (shapes of the wave packets are shown in Fig. 3c and 3d). The so-called full revivals are built at times close to  $t \simeq 20 T_{cl}$  and  $t \simeq 40 T_{cl}$  and a corresponding shape of the wave packet is exhibited in Fig. 3e.

Fig. 2 displays the same autocorrelation function (4) but in a much longer scale. The formation of recurrences corresponding to  $t_{sr}$  at  $t \simeq 300$  i.e.  $t = t_{sr}/3$  and to some extent to  $t \simeq 150$  i.e.  $t = t_{sr}/6$  respectively is clearly seen. The corresponding shape of the wave packet at first superrevival occurrence is present in Fig. 3f.

### 3 Spin–orbit pendulum

In this section we discuss the properties of the time evolution of wave packets representing a fermion moving in a spherical harmonic oscillator potential with a strong spin–orbit coupling. The hamiltonian of the system is then a simplified form of the single–particle Nilsson hamiltonian, extensively used in nuclear physics [24]

$$H = H_0 + V_{ls} = H_0 + \kappa (\vec{l} \cdot \vec{\sigma}) . \quad (5)$$

The extensive investigation of the problem is contained in refs. [18–21], here we review briefly the main results. In order to make the discussion simpler let us first focus attention on a particular case of circular orbits. Explicitly, we choose (without any loss of generality) the  $Oxy$  plane as the orbit plane and  $Ox$  as the initial spin direction (initial spin in orbit’s plane). Then the initial states take the following explicit form

$$|\Psi(t=0)\rangle = |N, \vec{x}\rangle = |N\rangle \frac{1}{\sqrt{2}} (|+\rangle + |-\rangle) , \quad (6)$$

where the eigenstate of  $s_x$  is expressed explicitly by the eigenstates of  $s_z$  operator ( $|+\rangle$  and  $|-\rangle$ ) and  $|N\rangle$  is the coherent state of spherical harmonic oscillator corresponding to a circular orbit. In configuration space it has the form

$$\langle \vec{r} | N \rangle = \pi^{-\frac{3}{4}} e^{-\frac{1}{2}[(x-x_0)^2+y^2+z^2]} e^{ip_0 y} . \quad (7)$$

This packet has its maximum at  $(x_0, 0, 0)$  and moves along the circular orbit if  $p_0 = x_0 = \sqrt{N}$ ,  $N$  – the average value of  $n$  quantum number (in this case average values of  $l_x, l_y, l_z$  are  $0, 0, x_0^2 = N$ , respectively). Note that the length of the angular momentum is also  $N$  in these units. The state  $|N\rangle$  can be decomposed in the HO basis as

$$|N\rangle = \sum_l \lambda_l |n=l, l, m=l\rangle = \sum_l \lambda_l |l l l\rangle , \quad (8)$$

i.e. it is a linear combination of states with  $m=l$  and  $n=l$ . This particular state which combines all the partial waves and consequently evolves during the time evolution with the spin–orbit coupling by using all the frequencies of the spin–orbit partners, can be taken as ‘pseudo’ one-dimensional harmonic

oscillator coherent state if one defines the weights  $\lambda_l$  in terms of  $l$  and a (continuous) real variable  $N$  as a Poisson distribution

$$|\lambda_l|^2 = e^{-N} \frac{N^l}{l!} . \quad (9)$$

As operators  $H_0$  and  $V_{ls}$  commute, the evolution operator connected with the Hamiltonian (5) can be factorized as

$$U(t) = U_0(t) U_{ls}(t) = e^{-itH_0} e^{-it(\vec{l} \cdot \vec{\sigma})} , \quad (10)$$

where the appropriate time units are chosen to absorb  $\kappa$  and  $\hbar$ . Using the equality  $(\vec{l} \cdot \vec{\sigma})^2 = l^2 - (\vec{l} \cdot \vec{\sigma})$  in the expansion of  $U_{ls}(t)$  one can rearrange it as

$$U_{ls}(t) = e^{-it(\vec{l} \cdot \vec{\sigma})} = f(t) + g(t)(\vec{l} \cdot \vec{\sigma}) , \quad (11)$$

where, with the initial condition  $U_{ls}(t=0) = 1$ ,

$$f(t) = e^{i\frac{t}{2}} \left[ \cos \Omega \frac{t}{2} - \frac{i}{\Omega} \sin \Omega \frac{t}{2} \right] , \quad (12)$$

$$g(t) = e^{i\frac{t}{2}} \left[ -\frac{2i}{\Omega} \sin \Omega \frac{t}{2} \right] . \quad (13)$$

In the last equations  $\Omega = \sqrt{1 + 4l^2}$  and states  $|lm\rangle$  are its eigenstates with the eigenvalues  $(2l + 1)$ .

The formulae (10–13) applied to (6) give the analytical form of the wave packet as a function of time. In the limit of high  $N$  (which in practice is achieved already for  $N \simeq 10$ ) we can provide a simple explanation of the dynamics. In this limit we obtain  $|\Psi(t)\rangle = |\Psi_+\rangle|+\rangle + |\Psi_-\rangle|-\rangle$  where the components of the spinor are given as

$$|\Psi_+\rangle = \frac{1}{\sqrt{2}} e^{-itH_0} \sum_l \lambda_l e^{-ilt} |lll\rangle , \quad (14)$$

and

$$|\Psi_-\rangle = \frac{1}{\sqrt{2}} e^{-itH_0} \sum_l \lambda_l e^{i(l+1)t} |lll\rangle . \quad (15)$$

Each component is again a coherent state that moves on a circular orbit of radius  $x_0$ , with angular velocities  $\omega_0 - \omega_{ls}$  and  $\omega_0 + \omega_{ls}$ , respectively. There is

in  $|\Psi_-\rangle$  an overall phase  $e^{it}$  which produces at time  $t = \frac{1}{2}T_{ls} = \pi$  the simple result  $|\Psi_-\rangle = -|\Psi_+\rangle$ , which means that a pure state with spin along  $-Ox$  is then observed.

These features are shown in details in Fig. 4 where the spatial motion of the wave packet (6-8) is plotted (more precisely only evolution under  $U_{ls}$  operator (11)). The figure displays the total probability density  $|\Psi(t)|^2$  for the case  $N = 18$  at times  $t_i = i/8 T_{ls}$ ,  $i = 0 - 4$ . As motion is periodic the motion in the second half of the  $T_{ls}$  period is symmetric to that of the first half. Fig. 5 illustrates the motion in the spin subspace. It displays time dependence of the  $\langle s_x \rangle$  and  $\text{Tr}(\rho^2)$ , where  $\rho$  is the density matrix reduced to the spin subspace. The oscillations of  $\langle \vec{s} \rangle$  are accompanied by the corresponding oscillations of  $\langle \vec{l} \rangle$  as the total angular momentum is conserved in the system. This effect of a periodic exchange of the portion of angular momentum between the spin and the ordinary subspaces has been called *spin-orbit pendulum* [18,19]. For analytical formulas and an extensive discussion see [18,19].

## 4 Time dependent vortex rings

In this section we want to discuss the same physical system with the hamiltonian (5) but quite different initial conditions corresponding to linear classical motion. More precisely we consider initial states in the form (6) but with the shape in configuration space at time  $t = 0$  given by

$$\langle \vec{r} | N \rangle = \pi^{-\frac{3}{4}} e^{-\frac{1}{2}[(x-x_0)^2 + y^2 + z^2]} . \quad (16)$$

This is the gaussian wave packet at rest centered at  $(x_0, 0, 0)$ ,  $x_0 = \sqrt{2N}$ , which in HO potential moves along  $Ox$  axis with average value of the angular momentum equal zero (note that according to (6) spin direction is the same). The decomposition into the HO basis is more general

$$|N\rangle = \sum_{nlm} \lambda_{nlm} |nlm\rangle . \quad (17)$$

The coefficients  $\lambda_{nlm}$  are known analytically for arbitrary initial conditions (for details see eq. (55) of ref. [21] and related discussion). Again with (10-13) and (17) one can derive the analytical formulas for the time evolution.

The details of this analytical formulation in terms of time dependent partial waves will be published elsewhere [25].

The examples of the motion of the wave packet with the lowest value of angular momentum ( $L = 0$ ) are shown in Figs. 6 and 7. Such a wave packet in absence of the spin-orbit coupling ( $\kappa = 0$ ) moves along the piece of the straight line on  $Oz$  axis. Both figures display only this part of the evolution which is governed by the  $U_{ls}$  operator, i.e. the harmonic oscillator motion is frozen. Both figures clearly show that the wave packet, initially well localized spreads into a torus (more precisely into two tori, the second with much lower density) with the classical trajectory being the symmetry axis. This spreading is reversible in our system due to its integrability and periodicity. Such 'vortex rings' topology of wave packets is presented here for the first time. The full motion is a superposition of spin-orbit motion and harmonic oscillator motion (10).

## 5 Conclusions

We have shown here that the presence of a spin-orbit interaction in a single-particle hamiltonian generates a new mechanism of collapses and revivals in wave packet dynamics. Assuming that initial state of a fermion is prepared in a form of a gaussian wave packet (a coherent state of harmonic oscillator) with well determined spin projection we are able to calculate its evolution in analytical terms. There exist some initial conditions for which formulas become compact and transparent, and can serve as a guidance for the most general cases. There are two extremes: the case  $N = L$  which corresponds to a circular classical orbit and the case  $L = 0$  corresponding to a linear orbit. In our simple model the constant form factor for spin-orbit coupling allows for a factorization of the evolution operator into two commuting parts. This fact makes possible considering both parts of the full motion separately and understand it better. The evolution operator  $U_{ls}$ , connected with the spin-orbit interaction results in splitting a wave packet into up and down components that evolve in a different manner. The so-called wave packet collapse reflects the vanishing overlap between subpackets. At  $(k + 1/2)T_{ls}$  the subpackets overlap again (exactly in the limit of high  $N$ ), with the opposite phases and the wave packet revives with spin reversed. At times  $kT_{ls}$  the subpackets overlap exactly with the same phases and the initial state is



exactly rebuilt. The sequence of collapses and revivals is accompanied by oscillations of average values of spin and orbital angular momentum, the so-called *spin-orbit pendulum* effect. This behaviour is common for any initial condition providing that spin is initially in orbit's plane.

In the hydrogenoid atoms it is necessary to combine the properties of Rydberg wave packets described in section 2 with the spin-orbit evolution that we have derived. In this way we obtain a complicated interference pattern in which the time scale due to the spin-orbit interaction must be included. No simple description has emerged yet.

## References

- [1] L.S. Brown, *Am. J. Phys.* **41** (1973) 525.
- [2] J. Parker and C.R. Stroud Jr., *Phys. Rev. Lett.* **56** (1986) 716.
- [3] I.S. Averbukh and N.F. Perelman, *Phys. Lett.* **A139** (1989) 449; *Zh. Eksp. Teor. Fiz.* **96** (1989) 818, (*Sov. Phys JETP* **69** (1989) 464); *Usp. Fiz. Nauk* **161** 41, (*Sov. Phys Usp.* **34** (1991) 572).
- [4] Z. Dačić-Gaeta and C.R. Stroud Jr., *Phys. Rev.* **A42** (1990) 6803.
- [5] A. Peres, *Phys. Rev.* **47** (1993) 5196.
- [6] J. Wals, H.H. Fielding and H.B. van Linden van den Heuvell, *Physica Scripta* **T58** (1995) 62.
- [7] R. Blum and V.A. Kostelecky, *Phys. Lett.* **A200** (1995) 308.
- [8] E.T. Jaynes and F.W. Cummings, *Proc. IEEE* **51** (1963) 129.
- [9] B. Buck and C.V. Sukumar, *Phys. Lett.* **A81** (1981) 132.
- [10] P.L. Knight, *Phys. Scripta* **T12** (1986) 51.
- [11] J. Gea-Banacloche, *Phys. Rev. Lett.* **65** (1990) 3385; *Phys. Rev.* **A44** (1991) 5913; *Opt. Commun.* **88** (1992) 531.
- [12] I.S. Averbukh, *Phys. Rev.* **A46** (1992) R2205.

- [13] D. Delande, J. Zakrzewski and A. Buchleitner, *Europhys. Lett.* **32** (1995) 107;  
A. Buchleitner and D. Delande, *Phys. Rev. Lett.* **75** (1995) 1487.
- [14] A.F. Brunello, T. Uzer and D. Farelly, *Phys. Rev. Lett.* **76** (1996) 2874.
- [15] I. Bialynicki-Birula, M. Kalinski and J.H. Eberly, *Phys. Rev. Lett.* **73** (1994) 1777;  
M. Kalinski, J.H. Eberly and I. Bialynicki-Birula *Phys. Rev.* **A52** (1995) 2460.
- [16] M.W. Noel and C.R. Stroud, Jr., *Phys. Rev. Lett.* **75** (1995) 1252.
- [17] E. Schrödinger, *Naturwissenschaften* **23** (1935) 807; **23** (1935) 823; **23** (1935) 844.
- [18] R. Arvieu and P. Rozmej, *Phys. Rev.* **A50** (1994) 4376.
- [19] P. Rozmej and R. Arvieu, *J.Phys.* **B29** (1996) 1339.
- [20] P. Rozmej and R. Arvieu, *Acta Phys. Polon.* **B27** (1996) 581.
- [21] R. Arvieu and P. Rozmej, *Phys. Rev.* **A51** (1995) 104.
- [22] R. Blum, V.A. Kosteletzky and J.A. Porter, *Am. J. Phys.* **64** (1996) 944.
- [23] I.C. Percival, *J. Math. Phys.* **2** (1961) 235.
- [24] S.G. Nilsson, *Kgl. Dansk. Vid. Selsk. Mat. Fys. Medd.* **16**, 29 (1955);  
S.G. Nilsson, C.F. Tsang, A. Sobiczewski, Z. Szymański, S. Wycech,  
G. Gustafsson, I.L. Lamm, P. Möller, B. Nilsson, *Nucl. Phys.* **A131**, 1 (1969).
- [25] R. Arvieu, P. Rozmej and W. Berej, submitted to *J. Phys. A*.

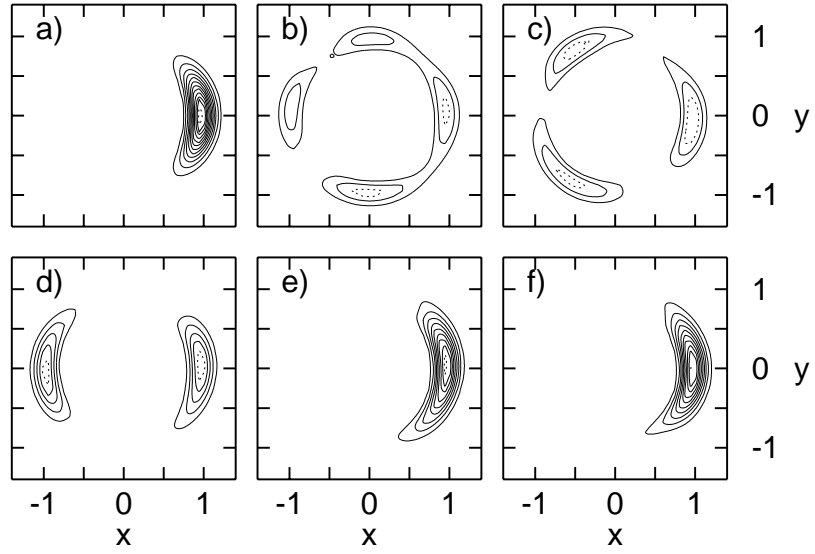


Figure 3:  
 Shapes of the wave packet (1) for  $t = 0, 4.97, 7.135, 9.964, 19.447, 298.333$  (case  $a, b, c, d, e, f$ , respectively). Time instants chosen for this presentation correspond to sharp peaks of the autocorrelation function (4) displayed in Figs. 1 and 2. Therefore the part of the wave packet (for fractional revivals) or the whole packet (for full revivals) is localized in the same position as the initial wave packet. Coordinates are in units equal to the radius of  $N$ th orbit.

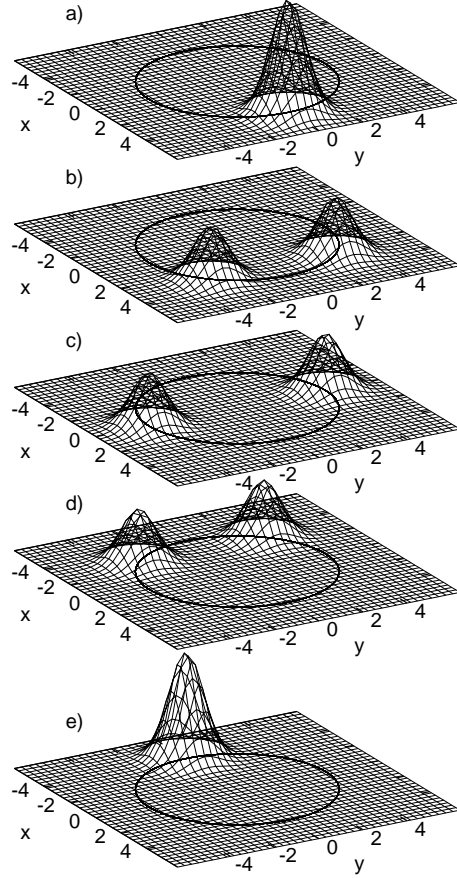


Figure 4: Motion of the circular wave packet with  $N = 18$  representing a fermion moving in the spherical harmonic oscillator potential with spin-orbit interaction (5). Shown is  $|\Psi(t)|^2 = |\Psi_+(t)|^2 + |\Psi_-(t)|^2$  on the plane of the classical orbit (marked by the circle) for  $t_i = i T_{ls}, i=0-4$  (from *a*) to *e*) in the reference frame moving like the classical particle (in other words presented is the evolution due to  $U_{ls}$  only).

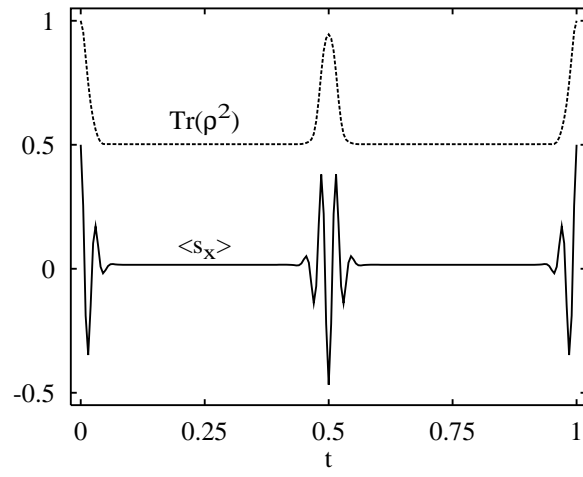


Figure 5: The time dependence of  $\langle s_x \rangle$  and  $\text{Tr}(\rho^2)$  ( $\rho$  - density matrix reduced to spin subspace). Time units equal to  $T_{ls}$ .

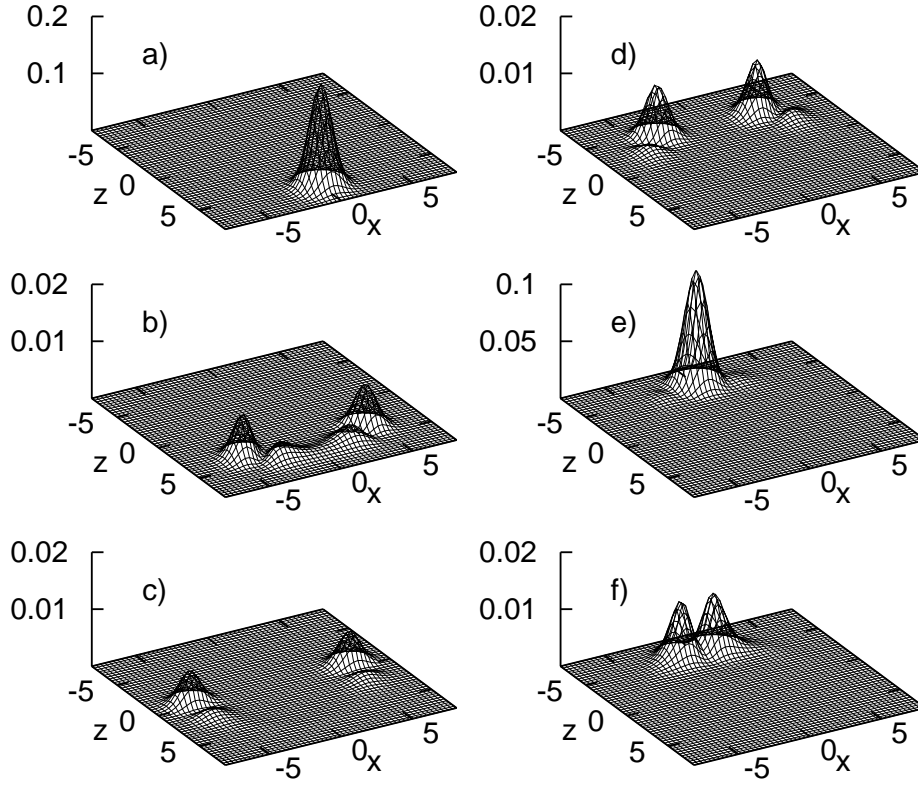


Figure 6: The same as in Fig. 4 but for initial conditions corresponding to the linear classical motion ( $N=18$ ,  $L=0$ ) along  $Oz$  axis. Shown is the probability density of the wave packet on the  $Oyz$  plane. The full 3-dimensional wave packet possesses the cylindrical symmetry around  $Oz$  axis. HO evolution is frozen as in Fig 4. Cases  $a, b, c, d, e, f$  correspond to  $t_i=0, 1/8, 2/8, 3/8, 7/16$  and  $4/8T_{ls}$ , respectively. Note different vertical scales.

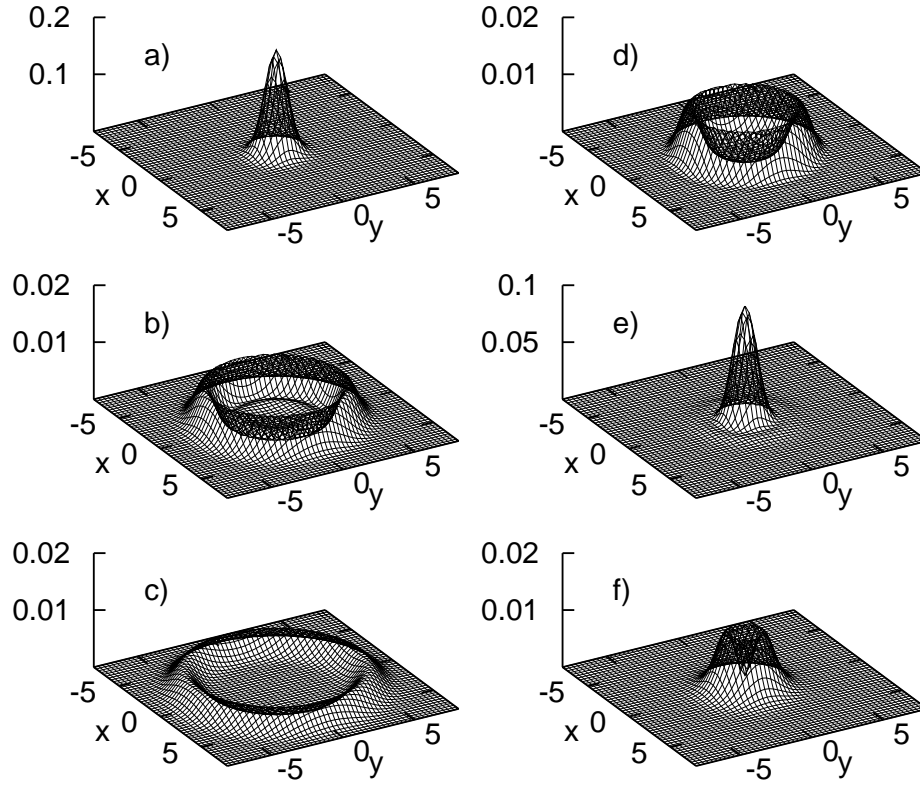


Figure 7: Cuts through the wave packet presented in Fig. 6 but by planes perpendicular to the symmetry axis with  $z = z_0 \cos t_i$  exhibiting a toroidal shape. Note different vertical scales. Time instants as in Fig. 6.

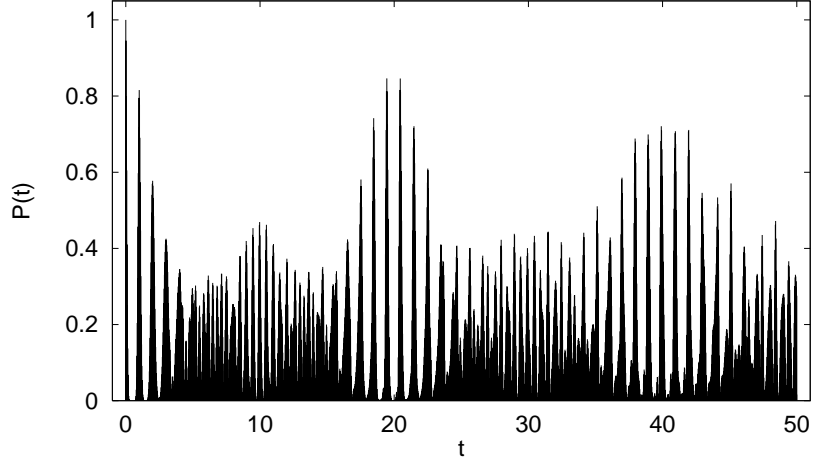


Figure 1: The recurrence probability (4) of the wave packet with  $N = 60$ ,  $\sigma = 1.5$  as function of time (time unit equal  $T_{cl}$  – the period of a classical revolution). It is easy to recognize the structures of full revivals at  $t \simeq 20, 40$  and fractional revivals at intermediate times.

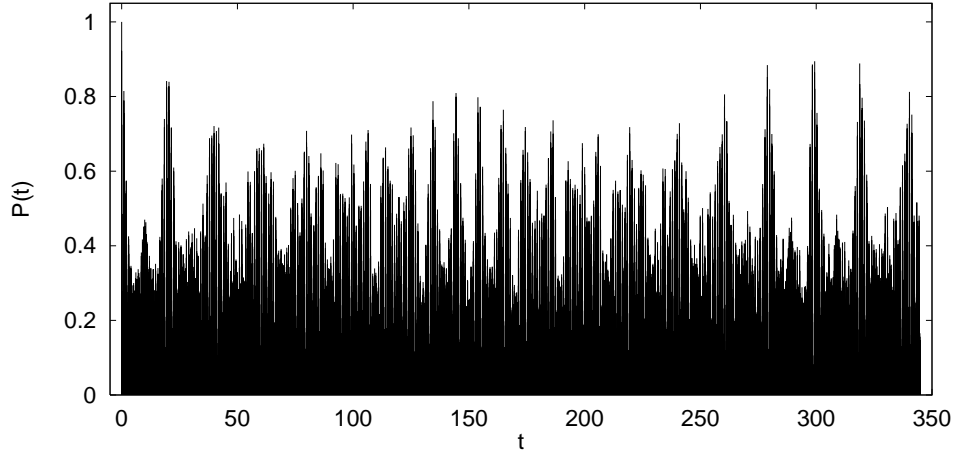


Figure 2: The same as in Fig. 1, but for much longer times. Strong recurrences at time  $t \simeq 300$  related to superrevival time  $t_{sr} \simeq 900$  are clearly visible.